HHS Public Access

Author manuscript

J Neuropathol Exp Neurol. Author manuscript; available in PMC 2015 May 12.

Published in final edited form as:

J Neuropathol Exp Neurol. 2011 August ; 70(8): 653–661. doi:10.1097/NEN.0b013e318225038c.

Targeting Vascular Amyloid in Arterioles of Alzheimer Disease Transgenic Mice with Amyloid Beta Protein Antibody-Coated Nanoparticles

Joseph F. Poduslo, PhD[a], **Kristi L. Hultman, PhD**[a], **Geoffry L. Curran, BS, MBA**[a], **Gregory M. Preboske, BS**[b], **Ryan Chamberlain, PhD**[c], **Małgorzata Marjańska, PhD**[c], **Michael Garwood, PhD**[c], **Clifford R. Jack Jr, MD**[b], and **Thomas M. Wengenack, PhD**[a]

[a]Departments of Neurology, Neuroscience, and Biochemistry/Molecular Biology, Mayo Clinic College of Medicine, Rochester, Minnesota

[b]Department of Radiology, Mayo Clinic College of Medicine, Rochester, Minnesota

[c]Center for Magnetic Resonance Research and Department of Radiology, University of Minnesota Medical School, Minneapolis, Minnesota

Abstract

The relevance of cerebral amyloid angiopathy (CAA) to the pathogenesis of Alzheimer disease (AD) and dementia in general emphasizes the importance of developing novel targeting approaches for detecting and treating cerebrovascular amyloid (CVA) deposits. We developed a nanoparticle-based technology that utilizes a monoclonal antibody against fibrillar human amyloid-β42 that is surface-coated onto a functionalized phospholipid monolayer. We demonstrate that this conjugated nanoparticle binds to CVA deposits in arterioles of AD transgenic mice (Tg2576) following infusion into the external carotid artery using 3 different approaches. The first 2 approaches utilize a blood vessel enrichment of homogenized brain and a leptomeningeal vessel preparation from thin tangential brain slices from the surface of the cerebral cortex. Targeting of CVA by the antibody-coated nanoparticle was visualized using fluorescent lissamine rhodamine-labeled phospholipids in the nanoparticles, which were compared with fluorescent staining of the endothelial cells and amyloid deposits utilizing confocal laser scanning microscopy. The third approach utilized high field strength magnetic resonance imaging of antibody-coated iron oxide nanoparticles (MIONs) following infusion into the external carotid artery. Dark foci of contrast enhancement in cortical arterioles were observed in T_2*-weighted images of ex vivo AD mouse brains that correlated histologically with CVA deposits. The targeting ability of these nanoparticles to CVA provides opportunities for the prevention and treatment of CAA.

Keywords

Alzheimer disease; Cerebral amyloid angiopathy; Cerebrovascular amyloid; Immunotargeted nanoparticles; Confocal laser scanning microscopy; Magnetic resonance imaging

Correspondence and reprint requests to: Joseph F. Poduslo, PhD, Mayo Clinic Rochester, 200 First Street SW, Rochester, MN 55905. Phone: (507) 284-1780; FAX: (507) 284-3383; poduslo.joseph@mayo.edu.

INTRODUCTION

Cerebrovascular amyloid (CVA) deposits are found in approximately 90% of patients with Alzheimer disease (AD), as well as sporadically in 30% of the population over the age of 60 (1, 2). Severe cases of familial cerebral amyloid angiopathy (CAA) also occur as the result of inherited point mutations in the amyloid precursor protein (APP), such as the Dutch and Flemish mutations. These cases exhibit increased levels of amyloid deposition in the vasculature in the absence of parenchymal amyloid plaques (3–5); affected persons develop substantial CAA and suffer from their first hemorrhagic stroke as early as their twenties (4).

CAA is characterized by deposition of amyloid-β (Aβ) peptides primarily in the media and adventitia of meningeal and cortical arteries and arterioles (6). The peptides are deposited mainly in vessel basal lamina and around smooth muscle cells (7–9). Amyloid deposition first occurs in pial arterioles in leptomeninges surrounding the cerebrum and appears to spread to more distal branches of the cortical arterioles, and then to the capillaries and vessels in other areas of the brain (3). Previous studies indicate that as the severity of the CVA deposition increases, the mechanical integrity of the vessel wall is compromised, resulting in an elevated risk of intracerebral bleeding, aneurysm formation, and hemorrhagic strokes (1, 10–12).

The development of targeted nanoparticles to CVA deposits could potentially aid in the diagnosis and, when available, treatment of vascular amyloid by allowing amyloid in the vessels to be distinguished from amyloid in parenchymal plaques. Our focus was on targeting CVA in isolated blood vessels and in surface leptomeningeal vessels using appropriate fluorescent markers. Detection by magnetic resonance imaging (MRI) utilized immunotargeted monocrystalline iron oxide nanoparticles (MIONs) that have the ability to target specific biomarkers in quantities detectable by MRI (13–15).

Previously, our group successfully targeted a novel monoclonal antibody IgG4.1, raised against human fibrillar Aβ42, to amyloid plaques in AD transgenic mouse brain (16). IgG4.1 binds specifically to the N-terminal of the Aβ peptide with preferential affinity towards fibrillar Aβ40 over monomeric Aβ40 peptides (17). Labeling amyloid plaques in the cortex and hippocampus of the brain requires that the compound successfully cross the blood-brain barrier (BBB), whereas labeling CVA deposits in leptomeningeal arteries and arterioles does not because of the absence of the BBB (18). Here, we report the development of IgG4.1 conjugated to nanoparticles to target CVA deposits and demonstrate our ability to detect the nanoparticle conjugates bound to CVA in AD mouse brains (Tg2576) ex vivo using confocal laser scanning microscopy and ultra-high field strength MRI following intra-carotid infusion.

MATERIALS AND METHODS

Preparation of Immunotargeted Iron Oxide Nanoparticles

Monodisperse γ-Fe_2O_3 nanoparticles (MIONs) approximately 8 nm in diameter were synthesized via a modified version of the Hyeon method (13, 19). First, a solution of 9.45 mmol oleic acid and 34.3 mmol trioctylamine was preheated to 200°C under an atmosphere

of nitrogen. Once the temperature of the solution stabilized, 3.04 mmol of $Fe(CO)_5$ were added, and the solution was refluxed for 24 minutes at 340°C. After cooling the solution below 130°C, 9.32 mmol of dehydrated trimethylamine-N-oxide was added. The nanoparticle solution was then heated to 130°C for 2 hours, followed by heating to 320°C for 1 hour. Finally, the solution was cooled to below 40°C and the nanoparticles were washed with ethanol and hexane. The nanoparticles were characterized for size, shape, crystallinity, and overall sample uniformity by transmission electron microscopy ([TEM], Jeol 1400), with an accelerating voltage of 100 kV. Only highly uniform, monocrystalline, monodisperse nanoparticle samples approximately 8 nm in diameter were used in the experiments.

Following characterization, the nanoparticles were coated with a 96:2:2 molar ratio of 1,2-distearoyl-sn-glycero-3-phosphoethanolamine-N-[methoxy(polyethylene glycol)-2000] (mPEG 2000), carboxylic acid functionalized mPEG 2000, and lissamine rhodamine tagged phosphatidylethanolamine phospholipids (Avanti Polar Lipids, Alabaster, AL) (13, 20). Briefly, a 400-μL sample of nanoparticles was precipitated in 1 mL of methanol and centrifuged. Following removal of the supernatant, the precipitated nanoparticles were allowed to dry for 20 minutes. The phospholipids were then dispersed in chloroform and added to the dried nanoparticles, and the solution was mixed thoroughly for 1 hour. The chloroform was then allowed to evaporate from the nanoparticle solution and 1.2 mL phosphate-buffered saline (PBS) was added. The solution was then centrifuged at 165,000 × *g* for 30 minutes to remove excess phospholipids and the nanoparticles were redispersed in PBS at a concentration of 10 mg/mL.

IgG4.1 mouse monoclonal antibodies raised against fibrillar human Aβ42 were then conjugated to the functionalized carboxylic acid groups of the phospholipids coating the nanoparticles using a carbodiimide reaction with the amine groups on the antibodies, thus producing IgG4.1-MIONs (16). This antibody binds specifically to the N-terminal of the Aβ peptide (residues 2–11); hence, it binds to both Aβ40 and Aβ42. To activate the nanoparticles for conjugation, 4 mg of 1-ethyl-3-[3-dimethylaminopropyl]carbodiimide hydrochloride (EDAC) and 4 mg of N-hydroxysulfosuccinimide (Sulfo-NHS) were added to 200 μL of MIONs, and the solution was mixed thoroughly for 15 minutes. The excess EDAC and Sulfo-NHS were then filtered out of the solution and 2 mg of IgG4.1 antibodies were added. The sample was then incubated at 4°C overnight, followed by purification to remove unconjugated antibodies using a 100-kDa MWCO centrifugal filtration device (Vivaspin). All other reagents were from Sigma (St. Louis, MO).

Animals and Experimental Procedures

Experiments were performed on 15- to 30-month-old B6SJL wild type (WT) and transgenic APP (Tg2576) mice. In our experience, CVA deposits begin at 15 months and progressively increase as the mice age. The mice were anesthetized using 1.5% isoflurane, and 150 μL of IgG4.1-nanoparticle (1 mg) were infused through a catheter into the left external carotid artery at a rate of 7.5 μL per min for 20 minutes. The catheter was positioned in the external carotid artery at the bifurcation with the internal carotid artery; hence, flow was directed from the common carotid into the internal carotid artery. The mice were then killed 20

minutes post-infusion following an overdose of sodium pentobarbital (200 mg/kg, i.p.). During the time interval of these experiments, the mice had no difficulty in tolerating the nanoparticle infusion. Seven to 10 AD and WT mice were used. Experimental animal procedures were approved by the Mayo Institutional Animal Care and Use Committee in accordance with the National Institutes of Health Guide for the Care and Use of Laboratory Animals.

Brain Tissue Preparation

For confocal laser scanning microscopy and TEM analysis of IgG4.1-nanoparticle binding to CVA deposits in cortical blood vessels, 2 techniques were used: 1) vessel enrichment of homogenized brain, and 2) leptomeningeal vessels in situ in thin tangential tissue slices from the surface of the cerebral cortex. To prepare the vessel enrichment from brain, the mice were perfused with PBS. The brains were removed and flash-frozen on dry ice. The brains were then homogenized in 1 mL of Tris EDTA sucrose buffer. The vessel fraction was separated from the homogenate using a 1.25 M and 1.5 M sucrose gradient and centrifuged at 58,000 × *g* for 1 hour (21). Brains used for tangential sectioning were fixed overnight in neutral-buffered, 10% formalin with the meninges intact. The next day, thin tangential slices of the leptomeningeal vessels and underlying tissue were dissected from the cortical surface.

TEM Analysis

For TEM imaging, both the vessel-enriched fraction and the leptomeningeal slices were incubated in Trump's reagent overnight and then embedded in epoxy resin. Ultra-thin sections were then cut and mounted on copper grids for imaging. The samples were imaged with a Jeol 1400 transmission electron microscope with an accelerating voltage of 100 kV.

Fluorescent Confocal Imaging

Targeting of CVA by the IgG4.1-nanoparticle conjugate was visualized using the fluorescent lissamine rhodamine labeled phospholipids in the coating of the nanoparticles, which was compared with fluorescent staining of the endothelial cells and amyloid deposits. Enriched vessel fractions and leptomeningeal vessel sections were incubated with a mouse monoclonal antibody to platelet endothelial cell adhesion molecule 1 (PECAM1) (Cat# CBL1337; Millipore; Billerica, MA) conjugated to Alexa Fluor 647 overnight to label the vascular endothelial cells. They were then rinsed with PBS and incubated with 1% aqueous thioflavine S for 5 minutes to label CVA deposits in the vessels; thioflavine S fluoresces green when bound to Aβ-pleated sheets. The tissue was then rinsed with PBS and ethanol and mounted on glass slides for fluorescent confocal imaging (Zeiss LSM 510). Control experiments performed with nanoparticles minus coated antibody showed no binding.

Ex Vivo MR Imaging

For ex vivo MRI experiments, the mice were killed with an overdose of sodium pentobarbital (200 mg/kg, i.p.) and perfused with PBS, followed by neutral-buffered, 10% formalin 20 minutes post-infusion. The brains were left in the skull and further fixed in formalin overnight before being embedded in 2% agar for imaging. MR images of the ex vivo samples were acquired at a resolution of 60 × 60 × 120 μm using 3-dimensional (3-D)

T_2*-weighted gradient-echo sequences. Images were acquired using a 9.4T, 31-cm horizontal bore magnet (Magnex Scientific, Oxford, UK) interfaced with a Varian INOVA MR console (Varian Inc., Palo Alto, CA) and a quadrature surface coil with 2 1-cm-diameter loops to transmit and receive radiofrequency signals. The acquisition parameters were as follows: repetition time (T_R) = 200 ms; variable echo time (T_E) ranging from 2.5 to 25.6 ms; and acquisition bandwidth = 117 kHz; flip angle = 52°.

Image Analysis

After ex vivo MRI, the brains were processed routinely for histology and stained for amyloid for correlation to the MR images to confirm labeling of amyloid by IgG4.1-MIONs. The bottom of the glass MRI tube was cut off and the agar and skull extruded. The brain was then dissected from the skull and cryoprotected in 10% followed by 30% sucrose in 0.1 M phosphate. After cryoprotection, frozen coronal sections (30 μm) were cut with a sliding microtome throughout the whole extent of the cerebral cortex. The sections were mounted on slides, dried, and then stained with fresh filtered aqueous 1% thioflavine S. The thioflavine S-positive amyloid deposits were visualized using fluorescence microscopy with settings for fluorescein isothiocyanate at an excitation wavelength of 488 nm and emission of 520 nm. Images of the thioflavine S-stained histological sections were co-registered with the MR images to identify colocalization of IgG4.1-MIONs with amyloid deposits using a 3-D voxel registration module in an image analysis software package (22).

RESULTS

Immunotargeting of IgG4.1-Nanoparticles to CVA in Enriched Blood Vessel Fractions from Homogenized Brain

Using triple staining, we demonstrated that the IgG4.1-nanoparticle conjugate bound to CVA in arterioles from the enriched blood vessel fractions of an APP mouse brain (Fig. 1a–d) but not WT mouse brain (Fig. 1e–h) following intra-carotid infusion. Blood vessels were labeled with an endothelial cell marker, anti-PECAM1 antibody conjugated to Alexa Fluor 647, and are shown in blue (Fig. 1c, d, g, h, false color); there was a diffuse pattern of labeling along the endothelial surface of the vessels. CVA deposits in the vessels were labeled with thioflavine S (Fig. 1b, d). As expected, the amyloid deposits in vessels from the APP mouse brain were located mainly in the arterioles in the basal lamina and around the smooth muscle cells; severely affected arterioles had a concentric ring-staining pattern. No CVA was detected in vessels from the WT mouse brain (Fig. 1f, h). The presence of the IgG4.1-nanoparticles was indicated by red fluorescence from the lissamine rhodamine tagged phospholipids coating the nanoparticles (Fig. 1a, d). The red fluorescence exhibited the same concentric ring pattern as seen with the thioflavine S staining, demonstrating the ability of the nanoparticles to pass through the endothelial layer and target the amyloid deposits around the smooth muscle cells. Colocalization of the IgG4.1- nanoparticles with the CVA deposits in the APP mouse brain vessels (indicated by the yellow and white areas on the composite image) demonstrated that the targeted nanoparticles bound specifically to the amyloid in the vessels (Fig. 1d). The very low level of red fluorescence in vessels from the WT mouse brain indicates that there was minimal non-specific binding of the IgG4.1-nanoparticles in the WT mouse brain vessels following intra-carotid infusion (Fig. 1e).

Immunotargeting of IgG4.1-Nanoparticles to CVA In Situ

Using triple staining on thin tangential slices of the cortical surface of the mouse brain, we demonstrated that the IgG4.1-nanoparticles targeted the CVA deposits in the basal lamina and around smooth muscle cells in the APP mouse brain, but did not bind to APP brain vessels devoid of amyloid deposits or to WT brain vessels. In the APP mouse, rings of red fluorescence indicated that the IgG4.1-nanoparticles bound to amyloid deposits around the smooth muscle cells (Fig. 2a, d), which colocalized with the thioflavine S amyloid staining (Fig. 2b, d). The distribution of the IgG4.1-nanoparticles and thioflavin S staining of amyloid were not entirely complementary, probably because the thioflavin S binds to β-sheet rich amyloid fibrils, whereas IgG4.1 binds to both diffuse and β-sheet containing amyloid (17). The IgG4.1-nanoparticles appeared to be able to pass through the endothelial cell layer of the arterioles because the nanoparticle labeling was observed in the abluminal side of the endothelium rather than colocalizing with the anti-PECAM1 labeling (Fig. 2a, c). The APP mouse brain vessel that exhibited no thioflavine S staining or indication of amyloid deposits (Fig. 2f) also exhibited no red fluorescence or targeting by the IgG4.1-nanoparticles (Fig. 2e). This vessel is most likely a venule in which we would expect no amyloid deposition. The WT mouse brain vessels exhibited no thioflavine S staining or IgG4.1-nanoparticle labeling (Fig. 2i, j, k, l).

Transmission Electron Microscopy

TEM analysis of the vessel-enriched samples and leptomeningeal tissue sections confirmed binding of the IgG4.1-nanoparticles to CVA deposits by direct visualization of the nanoparticles without the need of a secondary label. Staining of the vessel-enriched samples and leptomeningeal tissue sections with lead citrate was not used in order to enhance detection of nanoparticles, which are electron-dense because of their iron content and do not require staining. In the vessel-enriched samples of APP mouse brain, IgG4.1-nanoparticles were localized to amyloid deposits, appearing as small, dark uniform particles within the larger irregular patches (Fig. 3a, red arrows). As in the confocal images, no IgG4.1-nanoparticles were detected in the vessel-enriched sample from the WT mouse brains.

In tangential cortical tissue sections, nanoparticles were observed by TEM in association with amyloid deposits in blood vessel walls of APP mouse brain. The iron oxide nanoparticle cores of the IgG4.1-nanoparticles were only seen labeling amyloid deposits in the arterioles; thus, there was essentially no non-specific binding of the nanoparticles to the endothelium or other parts of the vessel walls (Fig. 3b, red arrows). The leptomeningeal arterioles in the WT mouse brains showed no sign of CVA deposits or IgG4.1-nanoparticle binding, as expected from the confocal images.

MR Imaging of IgG4.1-Nanoparticles in Ex Vivo Brain

While the majority of the CVA deposits are located in the leptomeningeal vessels, we focused on detecting the presence of CVA deposits in penetrating parenchymal cortical arterioles. Imaging the surface of the brain against the adjacent subdural space is complicated because of erosion of signal at the edge of the cortex due to magnetic susceptibility effect in MRI. Both short- and long-T_E MR images of WT and APP mouse brains were obtained ex vivo following intra-carotid infusion of IgG4.1-nanoparticles. In

WT brains, the cortex was a uniform gray due to the absence of amyloid plaques, particularly in the short-T_E MR image (Fig. 4a). Some slightly dark structures were visible in the long-T_E image of the WT mouse brain due to low levels of iron in oligodendrocytes in white matter tracts of the thalamus and corpus callosum (Fig. 4c). There was no evidence of contrast enhancement due to the presence of IgG4.1-nanoparticles in the brains of the WT mice. In the long-T_E images of the APP ex vivo brains, slightly dark foci appeared throughout the cortex and thalamus due to the presence of amyloid plaques (Fig. 4d, green arrows), which were also observed in non-infused APP mouse brain due to the presence of small amounts of iron in the amyloid plaques. In our experience, cortical amyloid plaques are not apparent in short-T_E MR scans due to reduced paramagnetic effects (Fig. 4b). Therefore, short-T_E MR scans were used to examine the targeting of the IgG4.1-nanoparticles to CVA in leptomeningeal vessels and cortical arterioles. Extremely dark foci indicating the presence of IgG4.1-nanoparticles were visible in both the short- and long-T_E MR images of the infused APP mice (Fig. 4b, d, red and blue arrows). No such foci were observed in the brains of WT mice, or in APP mice infused with unconjugated nanoparticles without IgG4.1. Some of the foci had the appearance of penetrating cortical arterioles due to their elongated radial structure perpendicular to the surface of the cortex (Fig. 4b, d, red arrows). The binding of the IgG4.1-nanoparticles were more apparent on the ipsilateral side of the brain, with a much lower level of targeting on the contralateral side of the brain.

Histological Confirmation of IgG4.1-Nanoparticle Binding to Amyloid Deposits in APP Mouse Brain

To correlate IgG4.1-nanoparticle MR contrast enhancement to histological structures routine processing and staining with thioflavine S were performed following *ex vivo* MRI of IgG4.1-nanoparticle-infused APP mouse brains. Thioflavine S labels both dense core amyloid plaques and CVA (Fig. 5). Contrast-enhanced dark foci in the cortex of the APP mouse brain in Figure 4 colocalize with amyloid deposits in a thioflavine S-stained histological section from the same dorsoventral region of cerebral cortex. Based on their morphology at high magnification, 2 of the deposits were blood vessels containing CVA (Fig. 4d, arrows 1 and 2). The third deposit is a cluster of amyloid plaques in close association with a blood vessel that is visible in an adjacent section. This might suggest dyshoric angiopathy in which flame-like amyloid deposits extend beyond the vessel wall and radiate into the neuropil (23). These observations confirm that IgG4.1-nanoparticles were not only able to label CVA in blood vessel walls of APP mouse brain, but also adjacent amyloid plaques in contact with CVA, which in turn suggests localized disruption of the BBB. Although evident in this figure, this was not frequently seen.

DISCUSSION

We have demonstrate the ability of the IgG4.1-nanoparticles to target CVA deposits in the brain arterioles of APP AD transgenic mouse brain and detected the presence of these nanoparticle MR contrast agents using standard MR imaging techniques. Using fluorescent confocal imaging and TEM, we have shown that the IgG4.1-nanoparticles specifically bind to the amyloid deposited around smooth muscle regions of the arterioles and that the nanoparticles are present in the vessels. Finally, we show the binding of the nanoparticles in

the vessels of APP mouse brain in concentrations detectable by MRI for the purpose of detecting CVA deposits in brain ex vivo and for distinguishing APP mice from normal WT mice.

The use of Aβ antibody-coated nanoparticles is restricted to the targeting of vascular amyloid to CVA deposits in arterioles. Leptomeningeal arterioles are fenestrated and hence have no BBB. The nanoparticles can readily diffuse through the arterioles to bind to the amyloid associated with the smooth muscle layer. In contrast, capillary CVA presents as linear thin layers of Aβ deposits in the perivascular basement membrane and as globular deposits of Aβ in the vessel wall. The permeability coefficient-surface area (PS) product for Aβ in AD transgenic mice at 52 weeks of age was not different than in WT mice (24); therefore, no BBB alterations are expected in brain capillaries at this age and our nanoparticles would not likely cross the capillary endothelial cell and target capillary CVA.

Brain arterioles contain endothelial cell tight junctions, but it is not clear whether these tight junctions form a barrier comparable to that of brain capillaries (25). The elimination of brain interstitial fluid and solutes is thought to involve the drainage pathway along basement membranes around capillaries and in the tunica media of arteries. Indeed, that fluorescent soluble tracers injected into the corpus striatum of mice spread diffusely through the brain parenchyma and then drain out of the brain along basement membranes of capillaries and arteries (26). It has been demonstrated, however, that the perivascular drainage of solutes is impaired in the presence of CAA (27). It is not clear whether our nanoparticles diffuse through the brain arteries and arterioles or follow the perivascular drainage pathway to target vascular amyloid.

Arteriolar CVA deposits likely affect smooth muscle contractility and hence arteriole blood flow and subsequent nutritional delivery. Indeed, an increased PS value to insulin in AD transgenic mice indicates a compensatory mechanism for enhanced delivery of insulin (24). Because insulin is taken up into the brain by a receptor-mediated transport system, these results suggest that there is an increase in insulin receptor density that compensates for the increase in CVA deposition. In contrast, the residual plasma volume for albumin is significantly increased in AD transgenic mice compared to normal adult mice, indicating increased adherence of albumin to the vessel walls (24). Because albumin (and IgG) are transported at the BBB by passive diffusion, increased amyloid deposition likely restricts their delivery into the brain and hence would directly affect the success of passive immunization. Therefore, prevention or removal of CVA at both the brain arteriole and capillary is an important therapeutic direction. By designing similar nanoparticles with an appropriate payload, it might be possible to deliver therapeutics to the arteriole CVA. Such agents might include antibodies against Aβ itself such as IgG4.1 or its $F(ab')_2$4.2 fragment (16), β-sheet breaker peptides (28) or other amyloid disruptors.

Acknowledgments

Support was provided by the Neuroscience Cores for MR Studies of the Brain from NINDS (NS057091), the Minnesota Partnership for Biotechnology and Medical Genomics, BTRC P41 RR008079, and the W. M. Keck Foundation.

References

1. Vinters HV. Cerebral amyloid angiopathy. A critical review. Stroke. 1987; 18:311–24. [PubMed: 3551211]
2. Jellinger KA. Alzheimer disease and cerebrovascular pathology: an update. J Neural Transm. 2002; 109:813–36. [PubMed: 12111471]
3. Maat-Schieman M, Roos R, van Duinen S. Hereditary cerebral hemorrhage with amyloidosis-Dutch type. Neuropathology. 2005; 25:288–97. [PubMed: 16382777]
4. Walker LC. Animal models of cerebral beta-amyloid angiopathy. Brain Res Brain Res Rev. 1997; 25:70–84. [PubMed: 9370051]
5. Levy E, Carman MD, Fernandez-Madrid IJ, et al. Mutation of the Alzheimer's disease amyloid gene in hereditary cerebral hemorrhage, Dutch type. Science. 1990; 248:1124–6. [PubMed: 2111584]
6. Weller RO, Nicoll JA. Cerebral amyloid angiopathy: pathogenesis and effects on the ageing and Alzheimer brain. Neurol Res. 2003; 25:611–6. [PubMed: 14503015]
7. Miyakawa T, Sumiyoshi S, Murayama E, et al. Ultrastructure of capillary plaque-like degeneration in senile dementia. Mechanism of amyloid production. Acta Neuropathol. 1974; 29:229–36. [PubMed: 4446949]
8. Perlmutter LS, Chui HC. Microangiopathy, the vascular basement membrane and Alzheimer's disease: a review. Brain Res Bull. 1990; 24:677–86. [PubMed: 2192775]
9. Yamaguchi H, Yamazaki T, Lemere CA, et al. Beta amyloid is focally deposited within the outer basement membrane in the amyloid angiopathy of Alzheimer's disease. An immunoelectron microscopic study. Am J Pathol. 1992; 141:249–59. [PubMed: 1632466]
10. Thomas T, Thomas G, McLendon C, et al. β-Amyloid-mediated vasoactivity and vascular endothelial damage. Nature. 1996; 380:168–71. [PubMed: 8600393]
11. Kase, CS. Cerebral Amyloid Angiopathy. In: Kase, CS.; Caplan, LR., editors. Intracerebral Hemorrhages. Boston: Butterworth-Heinmann; 1994. p. 179-200.
12. Okazaki H, Reagan TJ, Campbell RJ. Clinicopathologic studies of primary cerebral amyloid angiopathy. Mayo Clin Proc. 1979; 54:22–31. [PubMed: 759733]
13. Hultman KL, Raffo AJ, Grzenda AL, et al. Magnetic resonance imaging of major histocompatibility class II expression in the renal medulla using immunotargeted superparamagnetic iron oxide nanoparticles. ACS Nano. 2008; 2:477–84. [PubMed: 19206573]
14. Peng XH, Qian X, Mao H, et al. Targeted magnetic iron oxide nanoparticles for tumor imaging and therapy. Int J Nanomedicine. 2008; 3:311–21. [PubMed: 18990940]
15. Sun C, Fang C, Stephen Z, et al. Tumor-targeted drug delivery and MRI contrast enhancement by chlorotoxin-conjugated iron oxide nanoparticles. Nanomedicine (Lond). 2008; 3:495–505. [PubMed: 18694312]
16. Poduslo JF, Ramakrishnan M, Holasek SS, et al. In vivo targeting of antibody fragments to the nervous system for Alzheimer's disease immunotherapy and molecular imaging of amyloid plaques. J Neurochem. 2007; 102:420–33. [PubMed: 17596213]
17. Ramakrishnan M, Kandimalla KK, Wengenack TM, et al. Surface plasmon resonance binding kinetics of Alzheimer's disease amyloid beta peptide-capturing and plaque-binding monoclonal antibodies. Biochemistry. 2009; 48:10405–15. [PubMed: 19775170]
18. Ramakrishnan M, Wengenack TM, Kandimalla KK, et al. Selective contrast enhancement of individual Alzheimer's disease amyloid plaques using a polyamine and Gd-DOTA conjugated antibody fragment against fibrillar Abeta42 for magnetic resonance molecular imaging. Pharm Res. 2008; 25:1861–72. [PubMed: 18443900]
19. Hyeon T, Lee SS, Park J, et al. Synthesis of highly crystalline and monodisperse maghemite nanocrystallites without a size-selection process. J Am Chem Soc. 2001; 123:12798–801. [PubMed: 11749537]
20. Dubertret B, Skourides P, Norris DJ, et al. In vivo imaging of quantum dots encapsulated in phospholipid micelles. Science. 2002; 298:1759–62. [PubMed: 12459582]

21. Koide T, Gotoh O, Asano T, et al. Alterations of the eicosanoid synthetic capacity of rat brain microvessels following ischemia: relevance to ischemic brain edema. J Neurochem. 1985; 44:85–93. [PubMed: 3964837]

22. Robb, RA. A software system for interactive and quantitative analysis of biomedical images. In: Hohne, KH.; Fuchs, H.; Pizer, SM., editors. 3D Imaging in Medicine. Berlin-Heidelberg: Springer Verlag; 1990. p. 333-61.

23. Richard E, Carrano A, Hoozemans JJ, et al. Characteristics of dyshoric capillary cerebral amyloid angiopathy. J Neuropathol Exp Neurol. 2010; 69:1158–67. [PubMed: 20940625]

24. Poduslo JF, Curran GL, Wengenack TM, et al. Permeability of proteins at the blood-brain barrier in the normal adult mouse and double transgenic mouse model of Alzheimer's disease. Neurobiol Dis. 2001; 8:555–67. [PubMed: 11493021]

25. Nishizaki T, Matsuoka T. Low glucose enhances Na+/glucose transport in bovine brain artery endothelial cells. Stroke. 1998; 29:844–9. [PubMed: 9550521]

26. Carare RO, Bernardes-Silva M, Newman TA, et al. Solutes, but not cells, drain from the brain parenchyma along basement membranes of capillaries and arteries: significance for cerebral amyloid angiopathy and neuroimmunology. Neuropathol Appl Neurobiol. 2008; 34:131–44. [PubMed: 18208483]

27. Hawkes CA, Hartig W, Kacza J, et al. Perivascular drainage of solutes is impaired in the ageing mouse brain and in the presence of cerebral amyloid angiopathy. Acta Neuropathol. 2011; 121:431–43. [PubMed: 21259015]

28. Poduslo JF, Curran GL, Kumar A, et al. Beta-sheet breaker peptide inhibitor of Alzheimer's amyloidogenesis with increased blood-brain barrier permeability and resistance to proteolytic degradation in plasma. J Neurobiol. 1999; 39:371–82. [PubMed: 10363910]

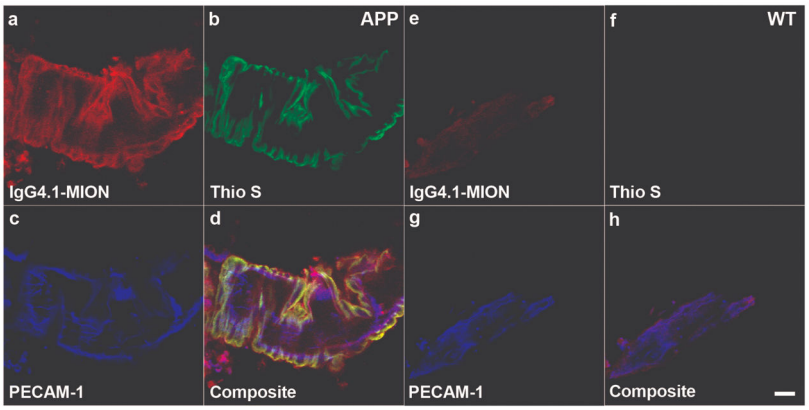

Figure 1.

Triple staining of enriched blood vessel fractions from amyloid precursor protein (APP) and wild type (WT) mouse brains following infusion of IgG4.1-nanoparticles into the external carotid artery. (**a**–**h**) IgG4.1-nanoparticles (MIONs) are apparent in a vessel from an APP mouse brain after infusion (red fluorescence - **a**, **d**), but not in a vessel from a WT mouse brain (**e**, **h**). Thioflavine S-stained cerebrovascular amyloid (CVA) deposits fluoresced green in a vessel from the APP mouse (**b**, **d**), but CVA was not present in vessels from the WT mouse (**f**, **h**). Anti-platelet endothelial cell adhesion molecule 1 (PECAM-1) antibody stained endothelial cells (blue) in vessels from both APP (**c, d**) and WT mice (**g, h**). The yellow color indicates colocalization of the IgG4.1-nanoparticles with amyloid deposits in a vessel from the APP mouse brain (**d**). Neither IgG4.1-nanoparticles nor CVA deposits are detected in vessels from the WT mouse brain (**e, f, h**). Scale bar = 25 μm (**h**).

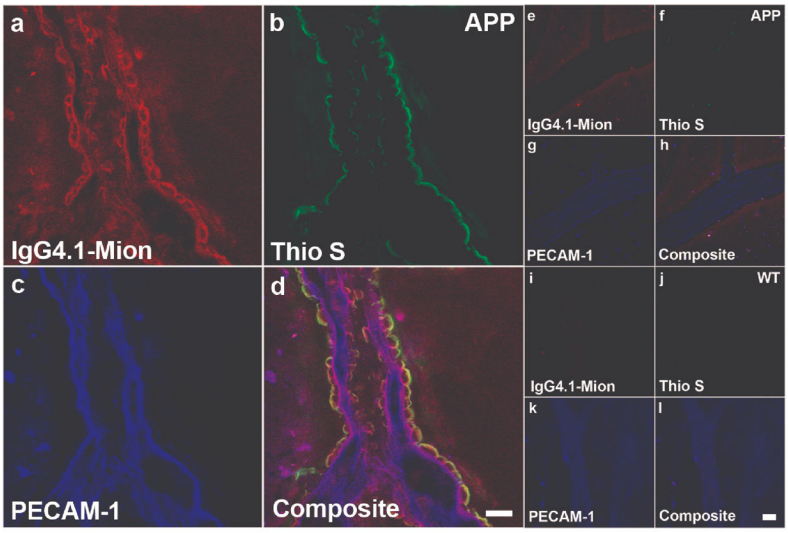

Figure 2.

Triple staining of leptomeningeal vessels in tangential tissue sections of cerebral cortex following infusion of IgG4.1-nanoparticles (MION) into the external carotid artery of amyloid precursor protein (APP) and wild type (WT) mice. (**a**–**l**) IgG4.1-nanoparticles are only apparent in vessels in the APP mouse brain (red fluorescence, **a**, **d**). Thioflavine S (Thio S)-stained cerebrovascular amyloid (CVA) deposits fluoresced green and are only present in vessels in the APP mouse brain (**b, d**). Anti-platelet endothelial cell adhesion molecules 1 (PECAM-1) antibody-stained endothelial cells are shown in blue (**c, d, g, h, k, l**). Yellow indicates colocalization of the IgG4.1-nanoparticles with amyloid deposits in a vessel in the APP mouse (**d**). A vessel without CVA in the APP mouse brain does not show targeting by the IgG4.1-nanoparticles (**e, f, h**). Neither IgG4.1-nanoparticles nor CVA deposits are detected in vessels from the WT mouse brain (**i, j, l**). Scale bars = 25 μm (**d, l**).

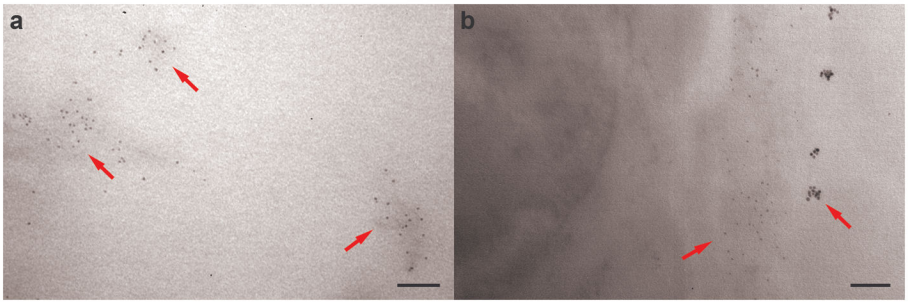

Figure 3.

Transmission electron microscopy image of IgG4.1-nanoparticles labeling amyloid deposits in a vessel-enriched homogenized brain sample (**a**) and within a leptomeningeal arteriole from a tangential section of cortex (**b**) of amyloid precursor protein (APP) mice infused with IgG4.1-nanoparticles. Red arrows indicate IgG4.1-nanoparticles (small, dark uniform particles) localized to amyloid deposits. Tissue was not stained to enhance visibility of electron-dense IgG4.1-nanoparticles. Scale bars = 100 nm (**a, b**).

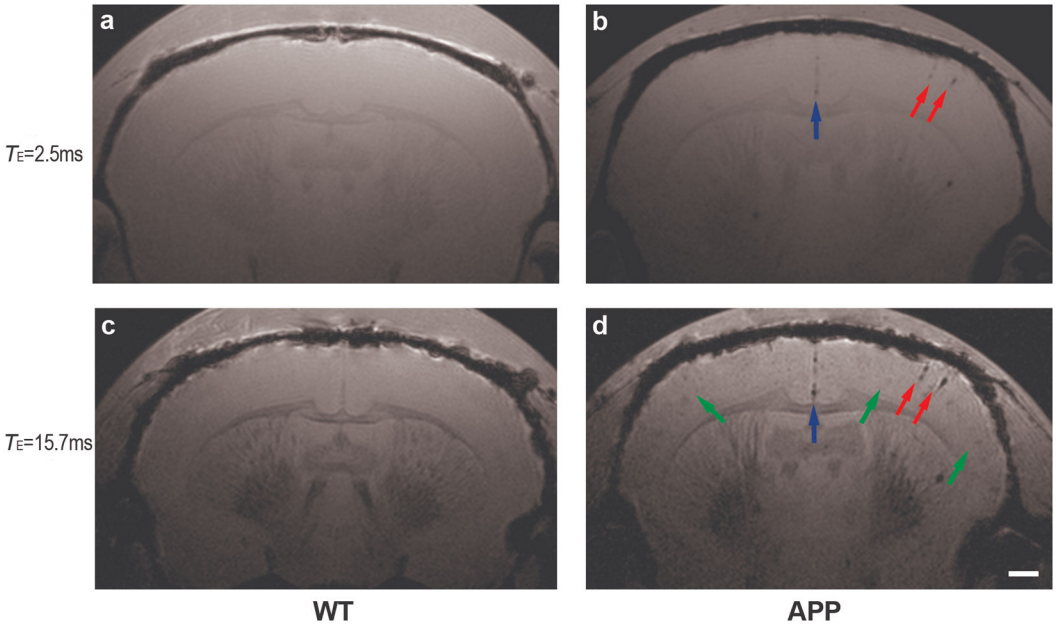

Figure 4.

Magnetic resonance images of wild type (WT) (**a, c**) and amyloid precursor protein (APP) (**b, d**) mouse brains ex vivo following infusion of IgG4.1-nanoparticles into the external carotid artery. In the long-T_E images (**c, d**), amyloid plaques in the APP brain appear as slightly dark foci in the cortex (**d**, green arrows), while the WT brain (**c**) is free of amyloid plaques and any dark foci in the cortex. In both the short- (**a, b**) and long-T_E images, IgG4.1-nanoparticle labeled cerebrovascular amyloid (CVA) deposits in cortical vessels in the APP brain appear as very dark foci (red arrows) on the infused side due to the strong paramagnetic effect of the iron oxide core (**b, d**). Cortical vessels in the WT brain are not visible due to the absence of CVA or nanoparticle-binding in the vessels. The dark foci along the center of the cortex in the APP mouse brain are the arterioles that contain CVA and are labeled with IgG4.1-nanoparticles (blue arrows, **b, d**). Scale bar = 500 μm (**d**).

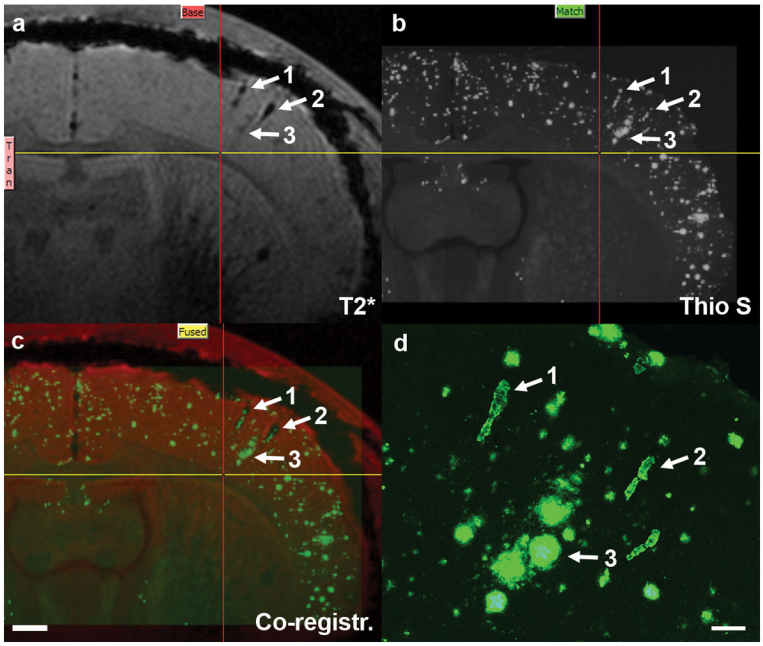

Figure 5.

Co-registration of long-T_E magnetic resonance (MR) image to corresponding thioflavine S-stained histological section of an amyloid precursor protein (APP) mouse brain after intra-carotid infusion with IgG4.1-nanoparticles, verifying IgG4.1-nanoparticle labeling of amyloid. (**a**) Long-T_E MR image from Figure 4d. (**b**) Corresponding histological section stained for amyloid with thioflavine S. Arrows indicate cerebrovascular amyloid (CVA) (1, 2 in figure) and amyloid plaques (3 in figure) labeled with IgG4.1-nanoparticles. Yellow and red lines mark same position in each panel for reference. (**c**) Result of 3-D voxel co-registration of images from **a** and **b** showing confirmation of labeling of amyloid deposits by IgG4.1-nanoparticles. Scale bar = 500 μm. (**d**) High magnification of structures labeled with arrows in **a**–**c** confirms that structures 1 and 2 are blood vessels containing CVA, based on their morphology. Structure 3 is a cluster of amyloid plaques in close association with a blood vessel that is visible in an adjacent section. Scale bar = 100 μm